arXiv:1601.06741v1 [astro-ph.GA] 25 Jan 2016

Astronomy Letters, 2016, Vol. 42, No. 3, pp. 182–192.

The z Distribution of Hydrogen Clouds and Masers with Kinematic Distances

V.V. Bobylev and A.T. Bajkova

Pulkovo Astronomical Observatory, St. Petersburg, Russia

Abstract—Data on HII regions, molecular clouds, and methanol masers have been used to estimate the Sun's distance from the symmetry plane $z_\odot$ and the vertical disk scale height h. Kinematic distance estimates are available for all objects in these samples. The Local-arm (Orion-arm) objects are shown to affect noticeably the pattern of the z distribution. The deviations from the distribution symmetry are particularly pronounced for the sample of masers with measured trigonometric parallaxes, where the fraction of Local-arm masers is large. The situation with the sample of HII regions in the solar neighborhood is similar. We have concluded that it is better to exclude the Local arm from consideration. Based on the model of a self-gravitating isothermal disk, we have obtained the following estimates from objects located in the inner region of the Galaxy ($R \leq R_0$) : $z_\odot = -5.7 \pm 0.5$ pc and $h_2 = 24.1 \pm 0.9$ pc from the sample of 639 methanol masers, $z_\odot = -7.6 \pm 0.4$ pc and $h_2 = 28.6 \pm 0.5$ pc from 878 HII regions, $z_\odot = -10.1 \pm 0.5$ pc and $h_2 = 28.2 \pm 0.6$ pc from 538 giant molecular clouds.

INTRODUCTION

The Galactic thin disk attracts the attention of many authors. Data on young O- and B-type stars, open clusters, Cepheids, infrared sources, molecular clouds, and other young objects are used to study its properties. In particular, such parameters as the Sun's distance from the symmetry plane $z_\odot$ and the vertical disk scale height h are important. Note that two terms are used: (a) the Sun's height above the Galactic plane and (b) the Sun's position relative to the symmetry plane. The Sun is known to slightly rise above the Galactic plane; therefore, the Sun's height is positive and is usually designated as $h_\odot$. In the heliocentric reference frame, the Sun's position relative to the symmetry plane of the Galaxy is calculated as the mean of the z coordinates of surrounding objects and, therefore, is negative at a positive height. This distance is usually designated as $z_\odot$.

The results of the analysis of samples with the distances estimated from trigonometric parallaxes (Maiz-Apellániz 2001), photometrically (Reed 2000), by analyzing open star clusters (Piskunov et al. 2006; Elias et al. 2006; Joshi 2007; Buckner and Froebrich 2014), or from a combination of various data (Bobylev and Bajkova 2016) are primarily of interest. At the same time, the less accurate kinematic distances have not lost their significance in analyzing the youngest disk objects, such as hydrogen clouds or methanol masers. Using such distances allows large samples of objects distributed almost over the entire Galactic disk to be analyzed (Bronfman et al. 2000; Fish et al. 2003; Paladini et al. 2004; Pandian et al. 2009).

Previously (Bobylev and Bajkova 2016), we estimated $z_\odot$ and h using OB associations, HII regions, Wolf–Rayet stars with known photometric distances, and a sample of classical Cepheids with their distances estimated from the period–luminosity relation. In addition, we used a sample of 90 masers with their trigonometric parallaxes measured by VLBI. The errors in these distances are very small, on average, 10%. However, when studying this sample, we found that the distribution of masers in a plane perpendicular to the Galactic plane has a noticeable asymmetry compared to the Gaussian one. In this paper, we want to ascertain what caused this asymmetry using various samples and various constraints. The goal of this paper is to minimize the influence of the main contributors (the Local arm and the Galactic disk warp) that give rise to an asymmetry in the z distribution of young Galactic-disk objects and to estimate the vertical disk scale height h. To solve this problem, we use a large statistical material from the compilation of Hou and Han (2014), which contains information about more than 2500 HII regions, 1300 giant molecular clouds, and 900 methanol masers with the estimates of their kinematic distances.

METHODS

In this paper, we use two rectangular coordinate systems: the moving heliocentric xyz and fixed Galactocentric XYZ ones. In the heliocentric xyz coordinate system, the x axis is directed toward the Galactic center, the y axis is in the direction of Galactic rotation, and the z axis is directed to the north Galactic pole. When we talk about the Galactic quadrants, we mean precisely this coordinate system. Thus, quadrants I, II, III, and IV span the ranges of Galactic longitudes $0^\circ < l \leq 90^\circ, 90^\circ < l \leq 180^\circ, 180^\circ < l \leq 270^\circ$, and $270^\circ < l \leq 360^\circ$, respectively.

In the Galactocentric XYZ coordinate system, the X axis is directed to the object from the Galactic center, the Y axis coincides with the direction of Galactic rotation, and the Z axis is directed toward the north Galactic pole. Here, it is important to know the Galactocentric distance R0 of the Sun. We use the present-day recent estimate of $R_0 = 8.34 \pm 0.16$ kpc obtained by Reid et al. (2014) from a large sample of Galactic masers with their trigonometric parallaxes measured by VLBI. In this coordinate system, it is convenient, for example, to draw the spiral pattern or to specify the inner ($R \leq R_0$) and outer ($R > R_0$) regions of the Galaxy.

In the case of an exponential density distribution, the observed histogram of the distribution of objects along the z coordinate axis is described by the expression

$$N(z) = N_1 \exp\Big(-\frac{|z - z_\odot|}{h_1}\Big), \tag{1}$$

where N_1 is the normalization coefficient and $z_\odot$ is the Sun's distance from the symmetry plane.

If the model of a self-gravitating isothermal disk is used for the density distribution, then the observed frequency distribution of objects along the z axis is described by

$$N(z) = N_2 \ \mathrm{sech}^2\Big(\frac{z - z_\odot}{\sqrt{2}\ h_2}\Big). \tag{2}$$

When comparing the results, it should be kept in mind that different authors use differing coefficients in the denominator when applying model (2): either two, $N(z) = N_2\ \mathrm{sech}^2[(z - z_\odot)/2h]$ (Maiz-Apellániz 2001; Buckner and Froebrich 2014), or one, $N(z) = N_2\ \mathrm{sech}^2[(z - z_\odot)/h]$ (Marshall et al. 2006).

Finally, the observed frequency distribution of objects along the z axis for the Gaussian model is described by the formula

$$N(z) = N_3 \exp\Big[-\frac{1}{2}\Big(\frac{z - z_\odot}{h_3}\Big)^2\Big]. \quad (3)$$

As was shown, for example, by Maiz-Apellániz (2001), h is determined with the smallest errors based on Eq. (2); therefore, this model is most attractive among the three described ones.

When analyzing the distributions of OB stars and open star clusters, many authors (Stothers and Frogel 1974; Reed 2000; Elias et al. 2006; Joshi 2007) made great efforts to rid the sample of the influence of the Gould Belt. An overview of the Gould-Belt properties can be found, for example, in Bobylev (2014). However, the fraction of Gould-Belt objects is quite small in the samples of HII regions or methanol masers. For example, only 12 masers in the sample of 130 masers with measured trigonometric parallaxes belong to the $r < 0.5$ kpc neighborhood, where the Gould Belt is located. However, the Gould Belt entirely belongs to a larger structure, the Local arm (Orion arm).

Previously (Bobylev and Bajkova 2016), we showed the z distribution of 130 masers with measured trigonometric parallaxes to be asymmetric. We suggested that this is because the sample is dominated by the masers observed mainly from the Earth's northern hemisphere. However, there can also be other sources of this peculiarity, which should be studied using a large statistical material. In particular, it is interesting to check the influence of the Local arm. As we showed previously (Bobylev and Bajkova 2014a), the symmetry plane of the Local arm has an inclination of about 6° to the Galactic plane. Since about 40 of the 130 masers belong to the Local arm, the effect here can be significant.

DATA

We use the data on ∼1800 HII regions, 1300 giant molecular clouds (GMCs), and ∼700 methanol masers from Hou and Han (2014), for which these authors estimated the distances kinematically. The distribution of all HII regions with available kinematic distance estimates in the Galactic XY plane is presented in Fig. 1, while the distribution of methanol masers and GMCs is presented in Fig. 2.

Figures 1 and 2 show a fragment of the global four-armed Galactic spiral pattern with a constant pitch angle of −13°. The pattern was constructed in our previous paper (Bobylev and Bajkova 2014b), where we analyzed the distribution of Galactic masers with measured trigonometric parallaxes, with the pattern parameters having been recalculated for the Galactocentric distance of the Sun adopted in this paper, $R_0 = 8.3$ kpc. As can be seen from these figures, the distribution of objects agrees satisfactorily with the plotted spiral pattern. In all samples, we see that the objects fall nicely on the segment of the Carina–Sagittarius arm (arm II in the figures) in forth quadrant. This is seen best in the

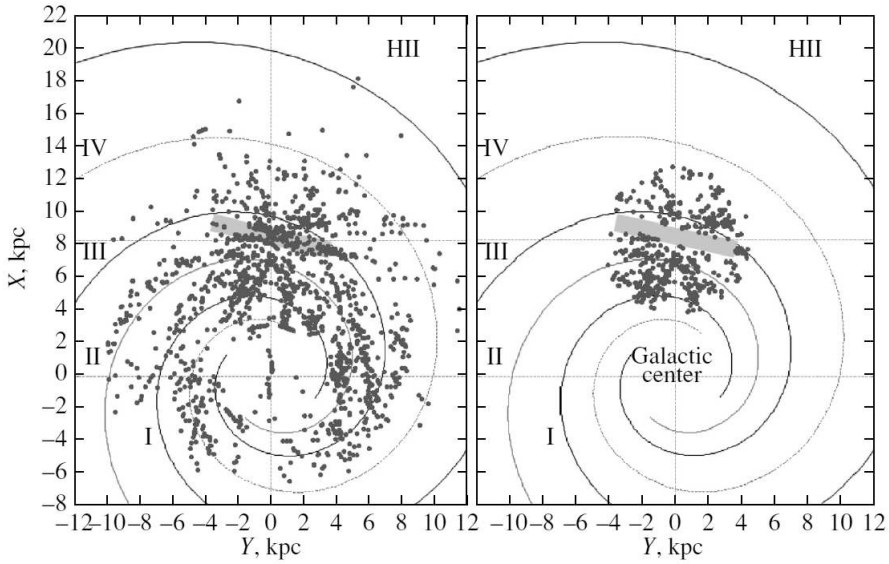

Figure 1: Distributions of the sample of 1771 HII regions (left) and the sample of 653 HII regions in the solar neighborhood, $r < 4.5$ kpc, without Local-arm objects (right) in the Galactic XY plane. The Sun's coordinates are $(X, Y) = (8.3, 0)$ kpc. The four-armed spiral pattern with a pitch angle of $-13°$ is plotted; the spiral arms are numbered by Roman numerals; the gray rectangle indicates the Local-arm model.

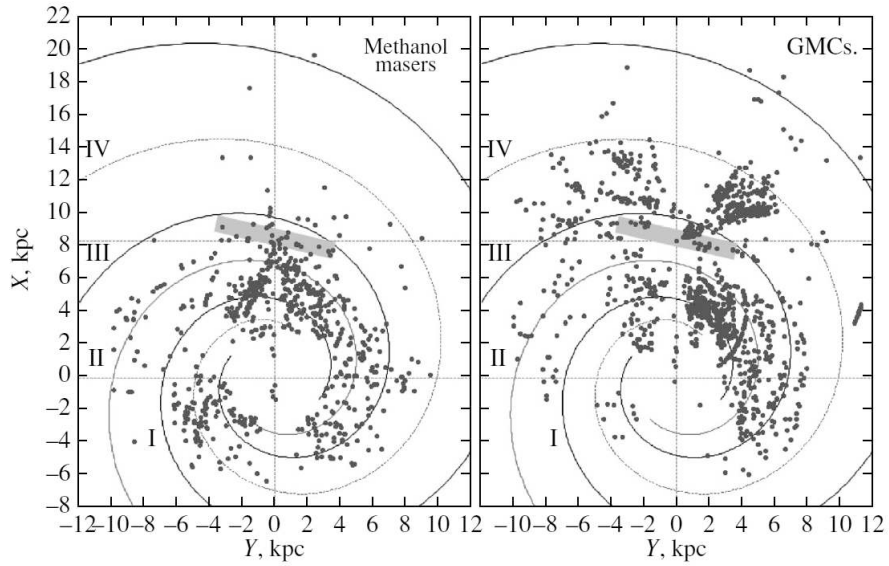

Figure 2: Distributions of the sample of 716 methanol masers (left) and the sample of 1281 giant molecular clouds (right) in the Galactic XY plane. The Sun's coordinates are $(X, Y) = (8.3, 0)$ kpc. The four-armed spiral pattern with a pitch angle of $-13°$ is plotted; the spiral arms are numbered by Roman numerals; the gray rectangle indicates the Local-arm model.

distribution of HII regions. Note that Hou and Han (2014) also reached the conclusion that the Galaxy most likely has a four-armed spiral pattern with a pitch angle of -13°. At the same time, they concluded that the model of a four-armed pattern with a variable pitch angle is even more suitable.

There are photometric distance estimates obtained by different authors for a relatively small number ($\sim$200) of HII regions in the compilation of Hou and Han (2014). These are objects fairly close to the Sun. Their distribution resembles the distribution of HII regions within 4.5 kpc of the Sun (the right panel in Fig. 1). Hou and Han (2014) added about a hundred more masers with measured trigonometric parallaxes to their sample of HII regions. These are not only methanol (CH_3OH) masers but also H_2O and SiO masers observed in the radio band at various frequencies using VLBI. The accuracy of such measurements is, on average, about 10%.

In this paper, we use a more complete sample of masers with measured trigonometric parallaxes that contains 130 sources. We compiled this sample based on a number of publications. The main work is the review by Reid et al. (2014), where the data on 103 masers are described. Subsequently, the publications of these authors with improvements and supplements devoted to the analysis of masers located in individual spiral arms of the Galaxy appeared. These include Sanna et al. (2014), Sato et al. (2014), Wu et al. (2014), Choi et al. (2014), and Hachisuka et al. (2015). Note the paper of Xu et al. (2013) devoted entirely to the masers in the Local arm. We used this sample of 130 masers previously (Bobylev and Bajkova 2016).

RESULTS

Influence of the Local Arm

As can be seen from Figs. 1 and 2, the Local arm is represented by a considerable number of objects only in the distribution of HII regions. In contrast, the number of Local-arm objects in the distribution of methanol masers is small, while there are virtually no Local-arm objects among the GMCs.

According to Bobylev and Bajkova (2014a), we took a 6.2×1.1 kpc rectangle oriented at an angle of -13° to the y axis and displaced from the Sun by 0.3 kpc toward the Galactic anticenter as the simplest Local-arm model. In accordance with this model, we cut out the HII regions on the right panel of Fig. 1, as marked by the gray rectangle located between the Perseus (arm III) and Carina–Sagittarius (arm II) arms.

Figure 3 presents the histograms of the z distribution for HII regions with kinematic distances and the sample of masers with measured trigonometric distances. The light shading on the left panel of the figure indicates the distribution for the sample of 653 HII regions from the $r < 4.5$ kpc solar neighborhood that contains no Local-arm objects, while the darker shading indicates the distribution of 134 HII regions belonging to the Local arm. The light shading on the right panel of the figure indicates the distribution for the sample of 88 masers that contains no Local-arm objects, while the thick line marks the distribution for the sample of 42 Local-arm masers.

Based on 653 HII regions from the $r < 4.5$ kpc solar neighborhood that contains no

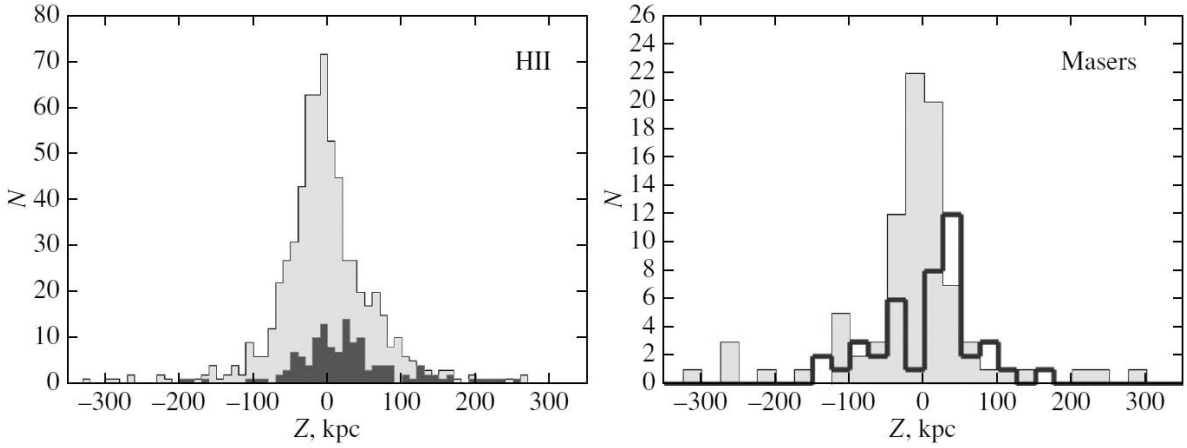

Figure 3: Histograms of the z distributions of HII regions and the sample of masers with measured trigonometric parallaxes. The dark shading on the left panel and the thick dark line on the right panel highlight the Local-arm objects.

Local-arm objects, we found

$$z_\odot = -5.1 \pm 2.6 \text{ pc}, \tag{4}$$

where $z_\odot$ was calculated as a simple mean, and its error was found as the error of the mean. Based on 134 HII regions belonging to the Local arm, we obtain

$$z_\odot = +26.7 \pm 6.5 \text{ pc}. \tag{5}$$

We can see a significant difference. We found

$$z_\odot = -14.3 \pm 11.6 \text{ pc}, \tag{6}$$

based on the sample of 88 masers (without any constraints on the distance from the Sun) that contains no Local-arm objects and

$$z_\odot = +4.7 \pm 9.9 \text{ pc}, \tag{7}$$

based on 42 Local-arm masers, and here the difference is also tangible. This difference is particularly clearly seen on the corresponding panel of Fig. 3. Finally, if the masers from the 0.5-kpc neighborhood (Gould-Belt masers) are rejected, then from the remaining 29 Local-arm masers we find

$$z_\odot = +23.6 \pm 12.6 \text{ pc}. \tag{8}$$

i.e., the entire Local arm gives a shift in the positive direction when calculating the mean $z_\odot$. Given the height of the Sun above the Galactic plane, we can conclude that the entire Local arm rises above the Galactic plane by about 25–35 pc.

Note that previously (Bobylev and Bajkova 2015) we revealed appreciable ($\sim$10 km s^{-1}) velocities in a direction perpendicular to the Galactic plane (the velocities W directed along the Z axis). The Galactic spiral density wave is probably responsible for such

periodic perturbations. The perturbations turned out to be particularly pronounced in the regions of the Gould Belt and the Orion and Perseus arms. On the whole, we can conclude that it is better not to use the Local-arm objects in the sample when analyzing the z distributions of stars. Below, we apply this rule to all our samples, in particular, to all samples in the table.

The $r < 4.5$ kpc Neighborhood

The table presents the results of determining the Sun's height $z_\odot$ and the vertical disk scale height $h_i, i = 1, 2, 3$ based on models (1), (2), and (3) using various samples of stars. These parameters and their errors were found by fitting the models to the histograms and Monte Carlo simulations. For this purpose, we constructed the histograms with a step in z of 10 pc. We assumed the errors in the distances determined kinematically to be 30% for all our samples. The upper part of the table presents the results obtained from the samples of objects that are located in the solar neighborhood with a radius of 4.5 kpc and contain no Local-arm objects.

Figure 4 presents the histograms of the z distributions for 240 masers, 653 HII regions, and 364 GMCs, where the curves of models (1) and (2) constructed with the parameters specified in the table are plotted. As can be seen from the figure, there is good agreement between the two model curves for all three samples. The distributions of masers and HII regions are quite symmetric and have no appreciable deviations from the Gaussian. In this regard, the distribution of GMCs appears farther from the Gaussian one, which may be because their longitude distribution is clumpy.

Figure 5 presents the longitude distribution of masers, HII regions, and GMCs. These are the samples used to find the parameters specified in the table and to construct Fig. 4. As can be seen from the figure, almost all of the masers lie at $|l| < 30^\circ$, because they are located in the inner region of the Galaxy. In the sample of masers, there is virtually no influence of the disk warp. In the two other samples, the influence of the disk warp manifests itself as a sine wave especially pronounced in the distribution of HII regions. This can be associated with large random errors in the distances. We used the constraint $r = 4.5$ kpc at which, as we expected, the influence of the disk warp should not be noticeable. However, because of the errors in the distance estimates (probably more than 30%), more distant objects that are significantly affected by the Galactic disk warp penetrated the sample.

The right panels of Fig. 5 present the Local-arm objects, while the probable members of the Gould Belt (selected from the solar neighborhood with a radius $r < 0.6$ kpc) are highlighted for the HII regions. As can be seen from the figure, HII regions are the most numerous members of the Local arm. 178 HII regions belong to the Local arm; 45 of them are located at $r < 0.6$ kpc. The fact that there are quite a few HII regions with large positive z in the range of longitudes $180^\circ < l < 240^\circ$ is unexpected. At least for the Gould-Belt objects in this range, one might expect negative z (as, for example, for the members of the Orion OB association). By contrast, the distribution of nearby GMCs that form two clumps near $l \approx 90^\circ$ and $l \approx 240^\circ$ agrees well with the expected picture.

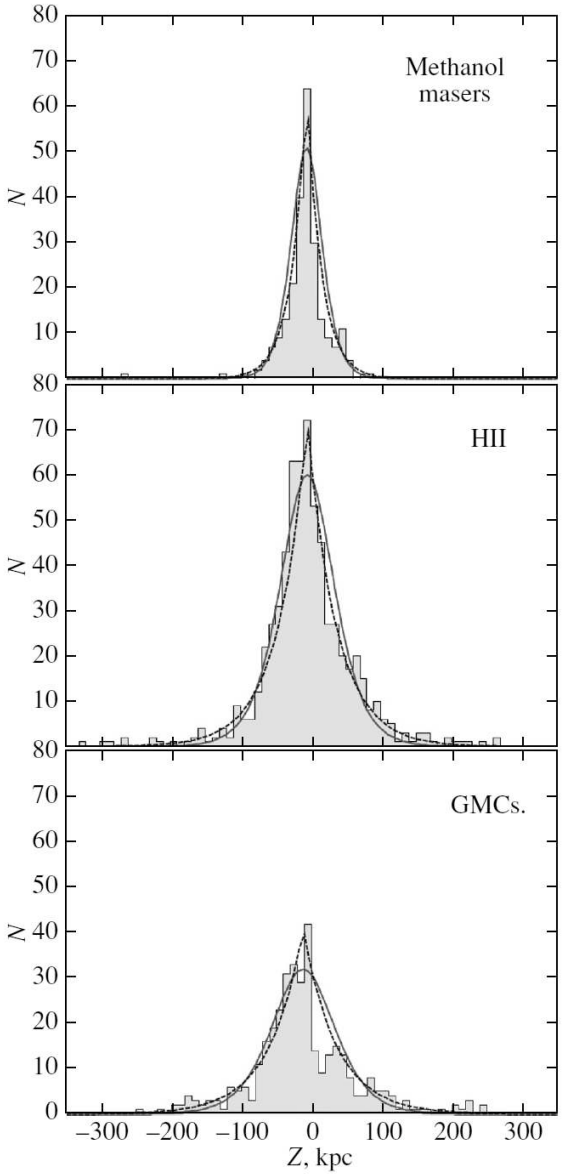

Figure 4: Histograms of the z distributions of 240 methanol masers (top), 653 HII regions (middle), and 364 giant molecular clouds (bottom). The dashed and solid lines on all panels represent models (1) and (2), respectively. All samples are located in the $r <$ 4.5 kpc neighborhood and contain no Local-arm objects.

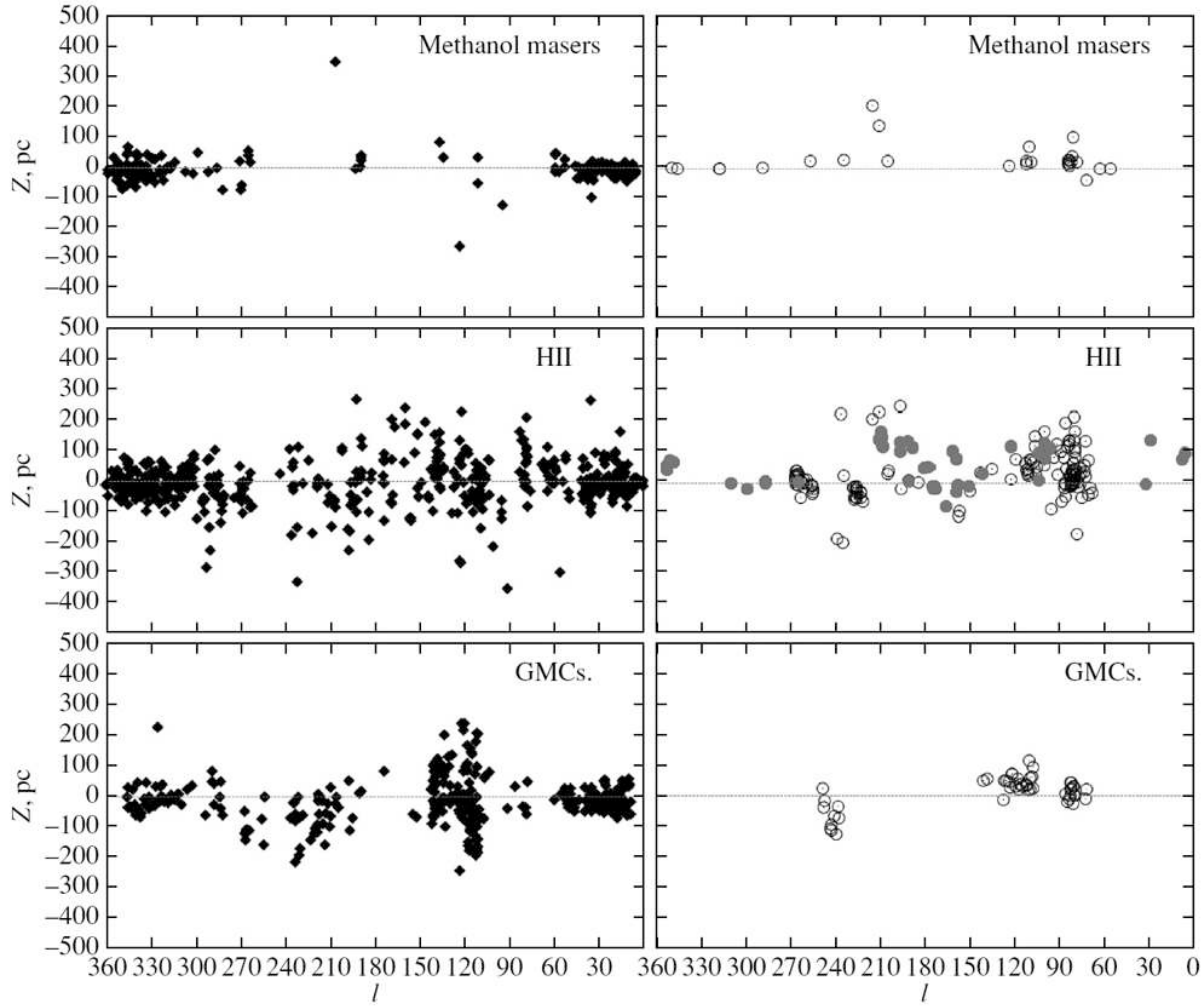

Figure 5: Longitude distributions of 240methanolmasers (top left), 653 HII regions (middle left), and 364 giant molecular clouds (bottom left). These samples are located in the $r < 4.5$ kpc solar neighborhood and contain no Local-Arm objects. The right panels present the Local-arm objects (open circles), while the probable Gould-Belt objects are highlighted (filled circles) for the HII regions.

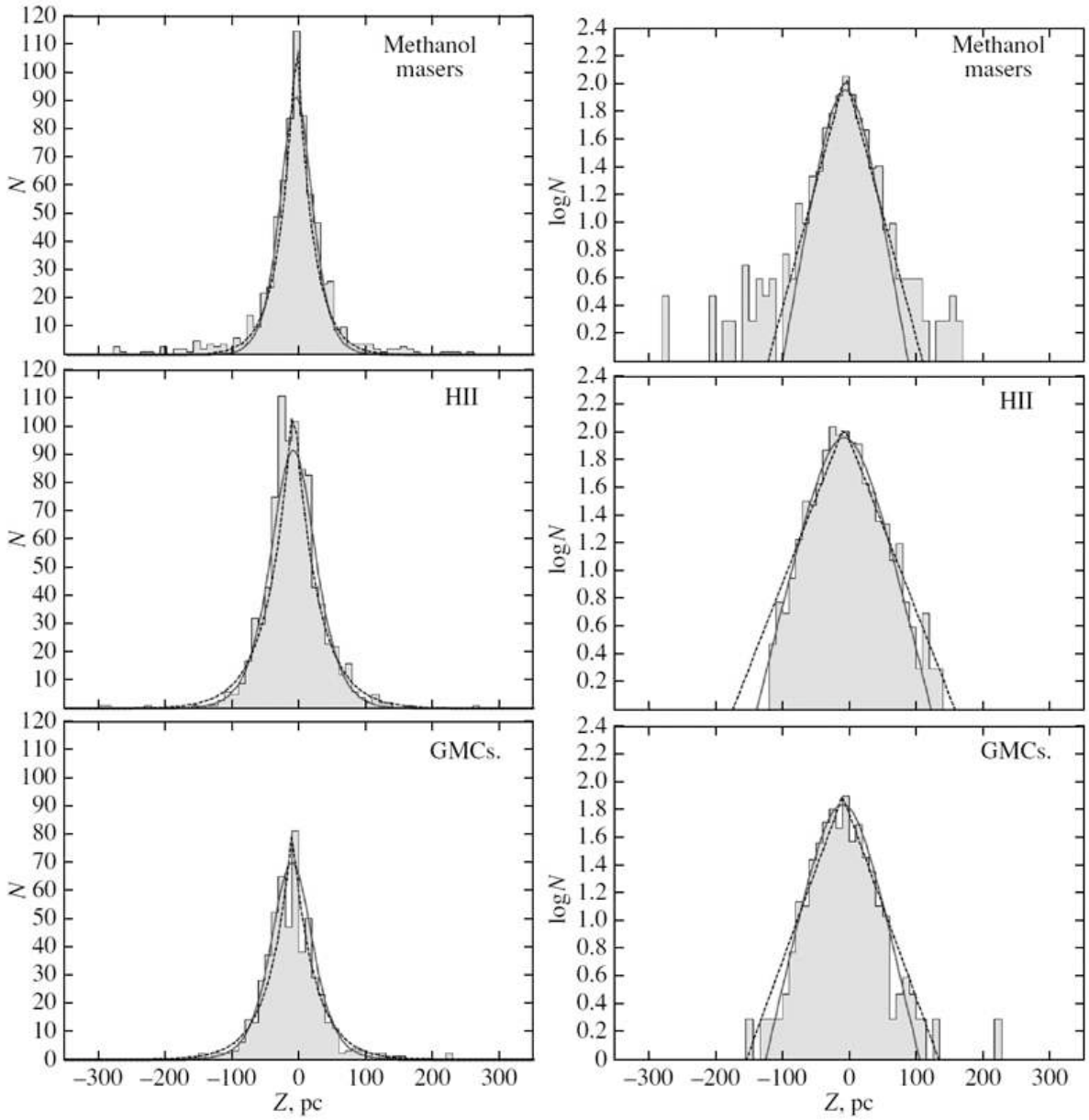

Figure 6: (a) Histograms of the z distributions of 639 methanol masers, 878 HII regions, and 538 GMCs from the inner region of the Galaxy. (b) The same histograms on a logarithmic scale. The dashed and solid lines on all panels represent models (1) and (2), respectively.

Table 1: The Sun's height $z_\odot$ and the vertical disk scale height $h_{i,\ i=1,2,3}$ obtained using models (1), (2), and (3) from three samples with kinematic distances

$z_\odot$, pc	h_1, pc	h_2, pc	h_3, pc	Sample
-6.4 ± 0.9	21.4 ± 1.1	20.7 ± 1.8	21.1 ± 1.4	240 masers, $r < 4.5$ kpc
-5.1 ± 0.8	41.5 ± 0.8	36.4 ± 0.7	42.0 ± 0.9	653 HII regions, $r < 4.5$ kpc
-12.2 ± 1.1	47.9 ± 1.5	42.6 ± 1.3	49.5 ± 1.6	364 GMCs, $r < 4.5$ kpc
-5.7 ± 0.5	26.5 ± 0.7	24.1 ± 0.9	25.9 ± 0.6	639 masers, $R \leq R_0$
-7.6 ± 0.4	32.8 ± 0.6	28.6 ± 0.5	33.0 ± 0.6	878 HII regions, $R \leq R_0$
-10.1 ± 0.5	33.8 ± 0.7	28.2 ± 0.6	32.5 ± 0.7	538 GMCs, $R \leq R_0$
$+0.9 \pm 1.8$	93.7 ± 2.6	83.9 ± 2.3	98.7 ± 2.9	380 HII regions, $R > R_0$
$+2.4 \pm 1.6$	110.5 ± 2.9	95.0 ± 2.3	110.1 ± 2.8	474 GMCs, $R > R_0$

The Inner and Outer Regions of the Galaxy

When analyzing the distances estimated kinematically from the Galactic rotation curve using the line-of-sight velocities, the separation into the inner and outer regions is justified by the form of errors. As Sofue (2011) showed, the distribution of errors in the distances when estimated via the line-of-sight velocities has a complex shape like a butterfly: its "body" located at the Galactic center is elongated in the Galactic center–Sun direction (the X axis), while its wings are elongated along the Y axis. The inner regions of the Galaxy have the smallest errors, except for the narrow zone around the tangential circumference.

Note that the XY distribution of almost the entire sample of methanol masers (Fig. 2) is close to the region of small errors in the kinematic distances. Almost the entire sample, 639 methanol masers, lies in the inner region of the galaxy, $R \leq R_0$. In contrast, there are few objects, about 130 masers, in the outer region of the Galaxy, $R > R_0$, and, therefore, we do not use them.

Figure 6 presents the histograms of the z distributions of 639 methanol masers, 878 HII regions, and 538 GMCs from the inner region of the Galaxy, $R \leq R_0$. The condition that allows the Local-arm region to be excluded was applied to all our samples. The criterion $r < 10$ kpc was additionally applied for the HII regions and GMCs, which allowed the very distant objects to be rejected. All three histograms in this figure are also presented on a logarithmic scale. The Sun's height and the vertical disk scale height obtained from all these samples are given in the middle and lower parts of the table.

Obviously, the results presented in the two lower rows of the table are far from the characteristics of the young disk. The positive $z_\odot$ and the huge h point to a very strong influence of the disk warp.

DISCUSSION

Comparison of the parameters presented in the table and the constructed z distributions in Figs. 4 and 6 shows an advantage of the samples located in the inner region of the

Galaxy. For example, the distribution of GMCs in Fig. 6 looks considerably more symmetric than that in Fig. 4; the distributions of HII regions and methanol masers became closer to the Gaussian. The closeness of the distributions to the theoretical ones specified by Eqs. (1), (2), and (3) was estimated each time using the χ^2 test from the formula $\chi^2 = \Sigma_i(\theta_i - \Phi_i)^2/\Phi_i$, where θ_i are the sampled values of the histogram normalized in such a way that $\Sigma_i\theta_i = 1$, Φ_i is the theoretical probability distribution that also obeys the normalization condition $\Sigma\Phi_i = 1$. For example, the χ^2 estimates for the approximations by distributions (1), (2), and (3) were 0.284, 0.837, and 0.999, respectively, for the sample of 364 GMCs (Fig. 4) and 0.197, 0.121, and 0.258 for the sample of 538 GMCs (Fig. 6). Comparison of these estimates suggests a more accurate approximation of the data by the theoretical distributions for the sample of 538 GMCs (Fig. 6) than that for the sample of 364 GMCs (Fig. 4). This is particularly clearly seen for the approximation by distribution (2).

The HII regions, giant molecular clouds, and methanol masers are intimately connected between themselves. All these objects are very young (approximately of the same age) and enter into star forming regions. One might expect the vertical disk scale heights found from these samples to be close. However, we can see such a situation only in the middle part of the table.

Note that many authors determined the Sun's height above the Galactic plane and the vertical disk scale height from various samples of HII regions and from molecular clouds. Masers were used much more rarely. Reviews of the $z_\odot$ and h determinations from various data can be found in Humphreys and Larsen (1995), Reed (2006), or Bobylev and Bajkova (2016). Therefore, the results that we obtained from a huge sample of methanol masers are of considerable interest. After all, methanol masers are associated with massive protostars in regions of active star formation, and, consequently, they reflect the distribution of just born massive stars.

Bronfman et al. (2000) studied the z distribution of 748 star-forming regions and H_2 clouds with available kinematic distances. These authors found $z_\odot \approx 5$ pc and $h \approx 40$ pc (here, h is the half-width at half maximum of the Gaussian distribution) from HII regions and $z_\odot \approx -6$ pc and $h \approx 60$ pc from molecular hydrogen clouds. They used the inner region of the Galaxy, $R/R_0 = 0.2 - 1.0$. Nevertheless, they found significant differences in the $z_\odot$ determinations from objects in quadrants I and II ($0^\circ < l < 180^\circ$) compared to objects in quadrants III and IV ($180^\circ < l < 360^\circ$). For example, they found $z_\odot = -12$ pc and $z_\odot = +3$ pc from northern- and southern-sky molecular clouds, respectively.

Based on a sample of 20 ultracompact HII regions, by first estimating their kinematic distances, Fish et al. (2003) found the vertical scale height to be 34.7 ± 1.4 pc (for the derived $z_\odot = -7.3 \pm 1.4$ pc). Note that the above scale height is the half-width at half maximum of the Gaussian.

Paladini et al. (2004) analyzed the z distribution of 550 HII regions. The distances to these regions were estimated in part kinematically from the Galactic rotation curve and in part based on the luminosity–diameter correlation. These authors found $z_\odot = -11.3$ pc and $h_3 = 52$ pc for the inner region of the Galaxy, $R < R_0$.

Pandian et al. (2009) determined the kinematic distances for 86 methanol masers and found the vertical scale heights of the masers to be $h_1 = 20$ pc ($z_\odot = -12.8$ pc) and $h_3 = 30$ pc ($z_\odot = -13.1$ pc). In their opinion, these vertical scale heights are considerably

smaller than those for the Galactic thin disk as a whole. Moreover, these authors also analyzed the z distribution for a sample of dark infrared clouds and found complete agreement of their h value with that found from masers.

Note the paper of Wienen et al. (2015), where the authors estimated the kinematic distances to 689 complexes of the ATLASGAL program (APEX Telescope Large Area Survey; the observations were performed at a wavelength of 870 mm) located in the first and fourth Galactic quadrants (almost all of them are located in the inner region of the Galaxy). The sources of this program are associated with massive cold clouds of dust located in regions of active star formation. It is important that a special technique that allows one to choose between the two alternative solutions (near or far distance) arising in this problem based on the character of spectral lines was applied in calculating the kinematic distances. A total of more than 1000 individual sources combined into complexes were used. The line-of-sight velocities were calculated as the mean from several molecular lines. Such measures allowed a high accuracy of the results to be achieved. These authors obtained the following estimates: $z_\odot = -7 \pm 1$ pc and $h_1 = 28 \pm 2$ pc.

We see that the spread in h is from 20 and 50 pc, and there are grounds for this spread: everything depends strongly on how the sources are distributed in the Galaxy. However, the minimum values of hi specified in the middle part of the table probably correspond best to the real picture.

The derived values of $z_\odot$ lying in the range from -6 to -10 pc are in good agreement with the results of other authors obtained from similar objects. At the same time, these values differ noticeably from the most probable estimates computed by using older objects (open star clusters, Cepheids, etc.). For example, previously (Bobylev and Bajkova 2016) we calculated the mean $z_\odot = -16 \pm 2$ pc based on the individual $z_\odot$ determinations from various samples.

We can conclude that our values of h obtained from the samples of HII regions, GMCs, and methanol masers (at $R \leq R_0$) reflect the character of the vertical scale height for the youngest stars in the Galaxy.

CONCLUSIONS

We obtained new estimates of the Sun's distance from the symmetry plane $z_\odot$ and the vertical disk scale height h using data on HII regions, giant molecular clouds, and methanol masers. For all these objects, there are distance estimates obtained by Hou and Han (2014) kinematically.

First, we showed that the entire structure of the Local arm affects noticeably the pattern of the distribution along an axis perpendicular to the Galactic plane. The entire Local arm rises above the Galactic plane by about 25–35 pc. The deviations from the distribution symmetry are particularly pronounced for the sample of masers with measured trigonometric parallaxes, where the fraction of Local-Arm masers is large. The situation with the sample of HII regions in the solar neighborhood is similar.

As a result, we concluded that it is better to exclude the Local-arm objects from consideration. Moreover, we found that the sough-for parameters were determined with the smallest errors from the objects located in the inner region of the Galaxy ($R \leq R_0$).

We applied three models of the density distribution to all three samples: an exponential distribution, a self-gravitating isothermal disk, and a Gaussian density distribution. All three models yield close values of h; therefore, we give only those found on the basis of the model of a self-gravitating isothermal disk. The following estimates were obtained from the objects located in the inner region of the Galaxy ($R \leq R_0$) : $z_\odot = -5.7 \pm 0.5$ pc and $h_2 = 24.1 \pm 0.9$ pc from the sample of 639 methanol masers, $z_\odot = -7.6 \pm 0.4$ pc and $h_2 = 28.6 \pm 0.5$ pc from 878 HII regions, and $z_\odot = -10.1 \pm 0.5$ pc and $h_2 = 28.2 \pm 0.6$ pc from 538 giant molecular clouds.

ACKNOWLEDGMENTS

We are grateful to the referees for their helpful remarks that contributed to an improvement of this paper. This work was supported by the "Transitional and Explosive Processes in Astrophysics" Program P–41 of the Presidium of Russian Academy of Sciences.

REFERENCES

1. V.V. Bobylev and A.T. Bajkova, Astron. Lett. 40, 783 (2014a).
2. V.V. Bobylev and A.T. Bajkova, Mon. Not. R. Astron. Soc. 437, 1549 (2014b).
3. V.V. Bobylev, Astrophysics 57, 583 (2014).
4. V.V. Bobylev and A.T. Bajkova, Mon. Not. R. Astron. Soc. 447, L50 (2015).
5. V.V. Bobylev et al., Astron. Lett. 42, 1 (2016).
6. L. Bronfman, S. Casassus, J.May, and L.-Å. Nyman, Astron. Astrophys. 358, 521 (2000).
7. A.S.M. Buckner and D. Froebrich, Mon. Not. R. Astron. Soc. 444, 290 (2014).
8. Y.K. Choi, K. Hachisuka, M.J. Reid, Y.Xu, A. Brunthaler, K.M. Menten, and T.M. Dame, Astrophys. J. 790, 99 (2014).
9. P.S. Conti and W.D. Vacca, Astron. J. 100, 431 (1990).
10. F. Elias, J. Cabrero-Caño, and E.J. Alfaro, Astron. J. 131, 2700 (2006).
11. V.L. Fish, M.J. Reid, and D.J. Wilner, Astrophys. J. 587, 701 (2003).
12. K. Hachisuka, Y.K. Choi, M.J. Reid, A. Brunthaler, K.M. Menten, A. Sanna, and T.M.Dame, Astrophys. J. 800, 2 (2015).
13. L.G. Hou and J.L. Han, Astron. Astrophys. 569, 125 (2014).
14. R.M. Humphreys and J.A. Larsen, Astron. J. 110, 2183 (1995).
15. Y.C. Joshi, Mon. Not. R. Astron. Soc. 378, 768 (2007).
16. J. Maiz-Apellániz, Astron. J. 121, 2737 (2001).
17. D.J. Marshall, A.C. Robin, C. Reylé, M. Schultheis, and S. Picaud, Astron. Astrophys. 453, 635 (2006).
18. R. Paladini, R.D. Davies, and G. DeZotti, Mon. Not. R. Astron. Soc. 347, 237 (2004).
19. J.D. Pandian, K.M. Menten, and P.F. Goldsmith, Astrophys. J. 706, 1609 (2009).
20. A.E. Piskunov, N.V. Kharchenko, S. Röser, E. Schilbach, and R.-D. Scholz, Astron. Astrophys. 445, 545 (2006).
21. B.C. Reed, Astron. J. 120, 314 (2000).
22. B.C. Reed, J.R. Astron. Soc. Canada 100, 146 (2006).
23. M.J. Reid, K.M. Menten, A. Brunthaler, X.W. Zheng, T.M. Dame, Y. Xu, Y.Wu, B. Zhang, A. Sanna, M. Sato, et al., Astrophys. J. 783, 130 (2014).
24. A. Sanna, M.J. Reid, K.M. Menten, T.M. Dame, B. Zhang, M. Sato, A. Brunthaler, L. Moscadelli, and K. Immer, Astrophys. J. 781, 108 (2014).

25. M. Sato, Y.W. Wu, K. Immer, B. Zhang, A. Sanna, M.J. Reid, T.M. Dame, A. Brunthaler, and K.M. Menten, Astrophys. J. 793, 72 (2014).

26. Y. Sofue, Publ. Astron. Soc. Jpn. 63, 813 (2011).

27. L. Spitzer, Astrophys. J. 95, 329 (1942).

28. R. Stothers and J.A. Frogel, Astron. J. 79, 456 (1974).

29. M. Wienen, F. Wyrowski, K.M. Menten, J.S. Urquhart, T. Csengeri, C.M. Walmsley, S. Bontemps, D. Russeil, at al., Astron. Astrophys. 579, 91 (2015).

30. Y.W. Wu, M. Sato, M.J. Reid, L. Moscadelli, B. Zhang, Y. Xu, A. Brunthaler, K.M. Menten, T.M. Dame, and X.W. Zheng, Astron. Astrophys. 566, 17 (2014).

31. Y. Xu, J.J. Li, M.J. Reid, X.W. Zheng, A. Brunthaler, L. Moscadelli, T.M. Dame, B. Zhang, Astrophys. J. 769, 15 (2013).